A Nonconformal Nonlocal Approach to Calculating Statistical Spread in Fatigue Indicator Parameters for Polycrystals

John Moore[1], Caitlin Martinez[1], and Ayushi Chandel[2]

[1]Marquette University
[2]Affiliation not available

January 27, 2024

Abstract

In the study of fatigue fracture in metals, fatigue indicator parameters (FIPs) are nonlocal quantities that are used to model and predict the driving force needed to incubate fatigue cracks. These FIP values can be used to design materials with microstructural features less prone to fatigue failure. However, the nonlocal nature of fatigue indicator parameters introduces another unknown variable that must be determined for accurate predictions: the volume over which nonlocal averages are performed. Many studies use nonlocal volumes that enclose a predetermined number of finite elements in a polygranular crystal plasticity simulation. To encapsulate the entire microstructure, these nonlocal volumes must be conformal to the microstructure (i.e., they do not overlap or have gaps between them). Some studies base the length scale of these nonlocal volumes on constant values or on the size of relevant microstructural features. It has been shown that if the length scale is too small, the nonlocal FIP predictions are mesh dependent. But, if the length scale is too large, the experimentally observed statistical spread in fatigue life is not captured. This work introduces a nonconformal nonlocal volume (i.e., a volume that surrounds each element and overlaps nonlocal volumes). Averaging FIP over this nonlocal volume both captures the spread in fatigue data and is mesh independent. It also allows for weighted nonlocal averages that would have excluded some of the microstructure using the conformal approach. While this approach is more accurate than the previous approaches, it does require a large amount of computational resources to determine each nonlocal volume, so a parallelized algorithm that is scalable across multiple computing nodes is employed. The example polycrystalline material for this work is Ti-6Al-4V, a common titanium alloy with a hexagonal closed-packed crystal structure.

Received: Added at production | Revised: Added at production | Accepted: Added at production

DOI: xxx/xxxx

TECHNICAL NOTE

A Nonconformal Nonlocal Approach to Calculating Statistical Spread in Fatigue Indicator Parameters for Polycrystals

John A. Moore | **Caitlin Martinez**

[1]Department of Mechanical Engineering, Marquette University, WI, USA

Correspondence
Corresponding author John A. Moore,
Email: john.a.moore@marquette.edu

Present address
Marquette University
Haggerty Hall
1515 W Wisconsin Ave
Milwaukee, WI 53233

Abstract

In the study of fatigue fracture in metals, fatigue indicator parameters (FIPs) are nonlocal quantities that are used to model and predict the driving force needed to incubate fatigue cracks. These FIP values can be used to design materials with microstructural features less prone to fatigue failure. However, the nonlocal nature of fatigue indicator parameters introduces another unknown variable that must be determined for accurate predictions: the volume over which nonlocal averages are performed. Many studies use nonlocal volumes that enclose a predetermined number of finite elements in a polygranular crystal plasticity simulation. To encapsulate the entire microstructure, these nonlocal volumes must be conformal to the microstructure (i.e., they do not overlap or have gaps between them). Some studies base the length scale of these nonlocal volumes on constant values or on the size of relevant microstructural features. It has been shown that if the length scale is too small, the nonlocal FIP predictions are mesh dependent. But, if the length scale is too large, the experimentally observed statistical spread in fatigue life is not captured. This work introduces a nonconformal nonlocal volume (i.e., a volume that surrounds each element and overlaps nonlocal volumes). Averaging FIP over this nonlocal volume both captures the spread in fatigue data and is mesh independent. It also allows for weighted nonlocal averages that would have excluded some of the microstructure using the conformal approach. While this approach is more accurate than the previous approaches, it does require a large amount of computational resources to determine each nonlocal volume, so a parallelized algorithm that is scalable across multiple computing nodes is employed. The example polycrystalline material for this work is Ti-6Al-4V, a common titanium alloy with a hexagonal closed-packed crystal structure.

KEYWORDS
Crystal Plasticity, Nonlocal Model, Probability and Statistics, Fatigue, Materials Design

1 | INTRODUCTION

1.1 | Overview

In the study of fatigue fracture in metals, fatigue indicator parameters (FIPs) are nonlocal quantities that represent the driving force to incubate fatigue cracks [1,2] and correlate well to crack tip opening displacement [3]. These FIP values can be used to design materials with microstructural features less prone to fatigue failure. [1,4,5,6,7]. However, the nonlocal nature of FIPs introduces another variables that must be determined for accurate predictions. Many studies use nonlocal volumes that enclose a predetermined number of finite elements [4,8,2,6,9]. To encapsulate the entire microstructure these nonlocal volumes must be conformal to the microstructure (i.e., they do not overlap or have gaps between them). These nonlocal volumes intrinsically have a length scale; some studies set a constant length scale [4,8,10] while others determine the length scale relative to the size of characteristic microstructural features [2,11,6,9]. It has been shown that if the length scale is too small, the nonlocal FIP data is mesh dependent. But, if the length scale is too large, the experimentally observed spread in fatigue life is not captured [11]. This work introduces a nonlocal nonconformal volume (i.e., a volume that surrounds each element, and overlaps nonlocal volumes). Averaging FIP over this nonlocal volume both captures the spread in fatigue data and is mesh independent. It also allows for weighted nonlocal averages that would have excluded some of the microstructure using the conformal approach. While this approach is more accurate than the

Abbreviations: FIP, fatigue indicator parameter, HCP, hexagonal close-packed, IP, in-plane direction, TT, through-thickness direction

previous approaches it does require a large amount of computational resources to determine each nonlocal volume, so a parallelized algorithm that is scalable across multiple computing nodes is employed. The example polycrystalline material for this work is Ti-6Al-4V, a common titanium alloy with a hexagonal closed-packed crystal structure.

1.2 | Background

It is common to use *S–N* or $\Delta\varepsilon^p$–*N* data ($\Delta\varepsilon^p/2$ is plastic strain amplitude and *S* is stress amplitude) to determine the number of mechanical load cycles until failure *N* of a material[9]. This is called the fatigue life of the material[9]. To fit a curve to the data, a power law is often used (for example, $\Delta\varepsilon^p = \mathcal{A}N^{\mathcal{B}}$, where $\mathcal{A}$ and $\mathcal{B}$ are parameters specific to a given material). To address different types of load states such as torsion or tension, different data sets and different curves are needed[12]. However, if fatigue life is not related directly to plastic strain or stress, but to a FIP then this load dependence is reduced. The relationship between FIPs and fatigue life often takes a power low form

$$FIP = AN^b, \tag{1}$$

where *A* and *b* are calibration parameters and the value of FIP is generally calculated based on the stress and strain state in the material.

Fatigue cracks nucleate, incubate, and the grow to small then large cracks; However the amount of cycles is not equal for each of these phases. Short or long crack growth has been observed to amount to a small percentage of the total fatigue life of a material[13,1]. The FIP determined here relates only to the crack life (*N*) prior to short or long crack growth (but should generally address a large percentage of the total life). Similar to the work in[6], this study will address incubation of cracks only, but this should be representative of the total life of the material.

For alloys, larger inclusions, defects, or grains that are oriented to favor plasticity tend to lower the fatigue life of the material. However, when calculating a FIP at the microscale using computational crystal plasticity and finite element models there is no intrinsic length scale associated with the model; and thus, FIPs do not automatically account for the size effect. Thus, McDowell et al.[14,15] introduced a length scale resulting in a non-local Fatemi-Socie FIP. Here a crystallographic version of the Fatemi-Socie FIP[16,11] is used and defined by

$$FIP^{(\alpha)} = \frac{\Delta\gamma_p^{(\alpha)}}{2}\left(1 + \kappa\frac{\sigma_n^{(\alpha)}}{\sigma_y}\right), \tag{2}$$

where, $\Delta\gamma_p^{(\alpha)}$ is the range of plastic shear strains over a cycle[1], $\sigma_n^{(\alpha)}$ is the stress perpendicular (i.e., normal) to a slip plane, all for a slip system α, σ_y is the yield strength. Fatemi and Socie[17] corrected for discrepancies between results from uniaxial and torsional loaded fatigue specimen via the constant κ. As shown by Eq. 2, the FIP value is determined for each slip system. In the work here, only the maximum FIP value over all the slip systems (at a given material point) is stored. In the work here κ is 0.55 (as used in[9]) and σ_y is 900 MPa (the average bulk yield strength given for Ti-6Al-4V in[18]). The plastic strain tensor $\boldsymbol{\varepsilon}^p$ is projecting the "onto the slip direction $\mathbf{s}^{(\alpha)}$ and slip plane normal $\mathbf{n}^{(\alpha)}$ respectively" to determine the plastic shear strain $\gamma_p^{(\alpha)}$[9]

$$\gamma_p^{(\alpha)} = \mathbf{s}^{(\alpha)} \cdot \boldsymbol{\varepsilon}^p \cdot \mathbf{n}^{(\alpha)}. \tag{3}$$

Similarly, Cauchy stress $\boldsymbol{\sigma}$ is projected onto a slip plane to determine the normal stress $\sigma_n^{(\alpha)}$

$$\sigma_n^{(\alpha)} = \mathbf{n}^{(\alpha)} \cdot \boldsymbol{\sigma} \cdot \mathbf{n}^{(\alpha)}. \tag{4}$$

To account for the size dependent relationship of of fatigue life on microstructure feature size, the FIP value in Eq. 2 is nonlocal. In the work here, every material point (integration point in finite element) is assigned a FIP and these are averaged over a nonlocal region similar to the average volume of the crystallographic grains (as in[11]).

Yet the shape of this region and how this nonlocal volume averaging is performed can take several forms. Castelluccio et al.[11] show that neglecting this nonlocal volume average—in a finite element simulation—results in a mesh dependent FIP value. They also consider averaging over crystallographic grains; this eliminates mesh dependence but reduces the spread in FIP values to an extent where it no longer represents fatigue statistics observed experimentally. This approach also does not hold the nonlocal volume constant, so microstructures with a wide distribution of grain sizes could result in very high FIPs in a few small grains.

Castelluccio et al. show that nonlocal volumes based on crystallographic slip planes result in both a realistic distribution of FIP and minimal mesh sensitivity. However, using as slip plane-based nonlocal volume requires predetermining the shape of a slip plane, which may become difficult for hexagonal close-packed (HCP) materials such as titanium where several slip planes carry the majority of the shear stress.

In Castelluccio et al.'s study, they show that nonlocal volumes that contain more than one crystallographic grain have advantages; they state that their "results demonstrate the limitation of using an apparent Schmid factor (considering only grain orientation and ignoring intergranular interactions) as a predictor of fatigue crack formation"[11].

Another disadvantage of nonlocal averaging over grains is that it does not address size effect; the model would produce the

same result with large or small grains (unless a size dependent constitutive law is implemented). Conversely, using a geometric nonlocal volume like a sphere or cube that is not based on the microstructure morphology allows the nonlocal volume to stay constant in size for large and small grains which in turn results in size effect.

Several studies use nonlocal volumes that contain more than one crystallographic grain; the studies in[4,8,2,6,9] predefine static nonlocal volumes for calculating FIP that are static (i.e., they do not move in the microstructure). This approach requires that all nonlocal volumes be conforming, such that there is no space in the microstructure where FIP is not averaged. It also does not allow for overlapping volumes.

Leblond, et al.[19,20] pose a nonlocal ductile fracture model that addresses unlimited localization in porous solids—where the microstructural defects are pores. They propose an averaging method for porosity that that is not uniform over a nonlocal volume and that "considerably improves numerical predictions". Reframing this approach in terms of FIP rather than porosity evolution rate gives

$$FIP^{\mathrm{nl}}(\boldsymbol{x}) = \frac{1}{A(\boldsymbol{x})} \int_{\Omega} \phi(\boldsymbol{x}-\boldsymbol{y}) FIP^{\mathrm{loc}}(\boldsymbol{y}) d\Omega, \tag{5}$$

where FIP^{loc} and FIP^{nl} are the local and nonlocal FIP values respectively. The position where the nonlocal FIP is calculated is $\boldsymbol{x}$ and $\boldsymbol{y}$ is positions around $\boldsymbol{x}$ over which FIP^{loc} is integrated. The nonlocal volume is Ω, and ϕ is a Gaussian distributed weighting function. The normalizing value of A is given by

$$A(\boldsymbol{x}) = \int_{\Omega} \phi(\boldsymbol{x}-\boldsymbol{y}) d\Omega, \tag{6}$$

and

$$\phi(\boldsymbol{x}) = \exp\left(-\|\boldsymbol{x}\|^2/l^2\right), \tag{7}$$

where l is the nonlocal length scale. For the work here, l is 13.37% of the length of the unit cell (which is based on achieving a nonlocal volume equal to the average grain volume).

If static conformal nonlocal volumes are used with the approach in Eq. 5, then regions near the edge of each volume carry a much lower weight than regions near the volume's centroid. However, there is no reason that some regions of the microstructure should be excluded in this way when calculating nonlocal FIP. To remedy this issue, the work here uses dynamic nonlocal volumes (i.e., that move with the location at which FIP^{loc} is calculated) and are nonconformal (i.e., each volume can overlap with other volumes). This means that unique spherical volumes surround each point $\boldsymbol{x}$ at which FIP^{loc} is calculated. So, every finite element has its own nonlocal volume. An illustration of these conformal and nonconformal nonlocal volumes are shown in Fig.1.

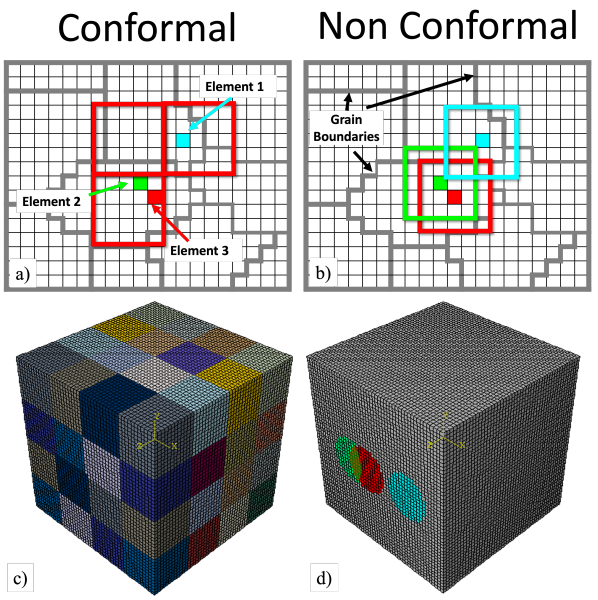

FIGURE 1 a) An illustration of a static conformal nonlocal volume (red boxes) around several finite elements in a polygranular microstructure b) An illustration of a three nonconformal nonlocal volumes (colored boxes corresponding to the element colors), notice that the nonlocal volumes overlap and are centered around each element c) Conformal nonlocal volumes in the $48 \times 48 \times 48$ element mesh d) Three example nonconformal nonlocal volumes in the $48 \times 48 \times 48$ element mesh (green, red, cyan circles), notice that the nonlocal volume can now be spherical as they do not need to be conformal and that they may overlap.

While these dynamic nonconformal nonlocal volumes reduce mesh dependence while maintaining the statistical spread in FIP seen experimentally and account for FIPs across grain boundaries, they require the determination of a large number of nonlocal volumes. For example, if a microstructural mesh has 100,000 elements then 100,000 nonlocal volumes are determined. For regular meshes, an algorithm can be formulated to efficiently determine these nonlocal volumes, but for irregular meshes these nonlocal volumes need formulated by systematically searching the mesh. For that reason, an approach based on Python parallel processing is proposed here. This approach is scalable across many processors and computing nodes.

Determining each nonlocal volume is an *embarrassingly* parallel task, so it can scale (nearly) linearly across a large number of computing cores and computing nodes on a high-performance computing cluster. Since Python's `multiprocessing` module[21], does not easily scale across several computing nodes, the work here uses the open-source Python library Dask[22] for parallelization of pre-processing scripts (specifically the `dask.distributed` library).

2 | MATERIALS & METHODS

2.1 | Micromechanics Model

The micromechanics model follows the derivation of[23] used in[6], only the key details of which are reproduced here. The deformation gradient of the material $\boldsymbol{F}$ is decomposed into an elastic $\boldsymbol{F}^e$ and plastic $\boldsymbol{F}^p$ part as

$$\boldsymbol{F} = \boldsymbol{F}^e \cdot \boldsymbol{F}^p. \tag{8}$$

This decomposition results in an *intermediate* configuration where the material has only partially deformed (i.e., plastic deformation but not elastic deformation). In this partially deformed configuration, the plastic velocity gradient $\tilde{\boldsymbol{L}}^p$ is determined by

$$\tilde{\boldsymbol{L}}^p = \sum_{\alpha=1}^{N_{slip}} \dot{\gamma}^{(\alpha)} (\tilde{\boldsymbol{s}}^{(\alpha)} \otimes \tilde{\boldsymbol{m}}^{(\alpha)}), \tag{9}$$

where N_{slip} is the number of slip systems, $\otimes$ is the tensor product, $\dot{\gamma}^{(\alpha)}$ is a shear strain rate at which slip occurs, $\tilde{\boldsymbol{s}}^{(\alpha)}$ is the direction of slip, and $\tilde{\boldsymbol{m}}^{(\alpha)}$ is the normal to the plane on which slip occurs, all for a crystal slip system (α). To determine the shear strain rate at which slip occurs, a rate dependent power-law approximates the relationship between stress and strain rate as

$$\dot{\gamma}^{(\alpha)} = \dot{\gamma}_0 \left| \frac{\tau^{(\alpha)} - a^{(\alpha)}}{\tau_0^{(\alpha)}} \right|^m \text{sign}(\tau^{(\alpha)}), \tag{10}$$

where m is a material parameter, τ_0 is a reference shear stress, $\dot{\gamma}_0$ is a reference shear strain rate, $a^{(\alpha)}$ is a backstress that describes kinematic hardening, and $\tau^{(\alpha)}$ is the resolved shear stress. The reference shear stress in each system is a weighting factor of a constant reference shear stress $\tau_0^{(\alpha)} = w\tau_0$ where w is a weighting factor and τ_0 is the constant reference shear stress. To determine the resolved shear stress $\tau^{(\alpha)}$, the Cauchy stress $\boldsymbol{\sigma}$ is projected onto $\boldsymbol{s}^{(\alpha)}$ and $\boldsymbol{m}^{(\alpha)}$ which are the slip direction and slip plane normal respectively using

$$\tau^{(\alpha)} = \boldsymbol{\sigma} : (\boldsymbol{s}^{(\alpha)} \otimes \boldsymbol{m}^{(\alpha)}), \tag{11}$$

where (:) is a double tensor contraction. Non-Schmid stresses that occur in titanium ,as shown in[24], are not addressed in the model. The reference shear stress τ_0 is a constant. The evolution of backstress $a^{(\alpha)}$ is determined by

$$\dot{a}^{(\alpha)} = h\dot{\gamma}^{(\alpha)} - ra|\dot{\gamma}^{(\alpha)}|, \tag{12}$$

where the direct and dynamic hardening factors are h and r respectively.

Four families of slip systems in the HCP α phase are considered. These families are: basal, prismatic, pyramidal $\langle \boldsymbol{a} \rangle$ and pyramidal $\langle \boldsymbol{c} + \boldsymbol{a} \rangle$. The weighting factors w for the basal, prismatic, pyramidal $\langle \boldsymbol{a} \rangle$ and pyramidal $\langle \boldsymbol{c} + \boldsymbol{a} \rangle$ families are 1.0, 1.0, 1.13, and 2.12 respectively. The first three weights are used in[25] and the pyramidal $\langle \boldsymbol{c} + \boldsymbol{a} \rangle$ weight is determined to match the anisotropy of the material shown in[26]. The $\langle \boldsymbol{c} \rangle$ to $\langle \boldsymbol{a} \rangle$ ratio is 1.599.

Only the α phase is modeled, rather than the α and β phase together[24,25]. While this is an approximation,[25] shows that the main effect of the β is on the elasto-plastic transient regime between full elasticity and full plasticity, so the error in predicting stress–strain response is minimal using this assumption.

2.2 | Finite Element Model

The finite element model uses four different meshes ranging from coarse to fine based on the mesh sizes used in[11]. These meshes are $11 \times 11 \times 11$, $19 \times 19 \times 19$, $32 \times 32 \times 32$, and $48 \times 48 \times 48$ elements respectively and are shown in Fig.2. Reduced integration hexahedral finite elements with eight nodes per element are used exclusively for implicit simulations using Abaqus (2018) finite element software. Displacement boundary conditions are applied on faces with normals in the negative directions. Faces with normals in the x-, y-, and, z-directions receive only displacement constraints parallel to each face normal. Constraint equations are used to enforce periodicity by holding each free face flat. A displacement is applied to the microstructure in the x-direction; subsequently, the displacement in the y- and z-directions contracts or extends based on the apparent Poisson's ratio of the material. Each microstructure mesh is loaded cyclically for three full cycles and a strain amplitude of 0.5% and an R ratio of –1. This amounts to a maximum and minimum average stress of approximately $\pm$600 MPa.

Fifty different realizations of microstructures are used for each mesh. Each realization has 100 randomly distributed equiaxed crystallographic grains with a constant Euler angle for each grain. The crystallographic texture is random. So, each realization has both a unique random texture and random grain structure. The grain morphology for each microstructure realization is created using tessellation in the software Neper[27,28,29].

The elastic parameters in Voigt notation are C_{11} = 162400 MPa, C_{12} = 92000 MPa, C_{44} = 69000 MPa. The material parameters used in the simulations are shown in Tab.1. These parameters are calibrated to data from[26] and the resulting comparison to the anisotropic Ti-6Al-4V data from[26] is shown in Fig.3.

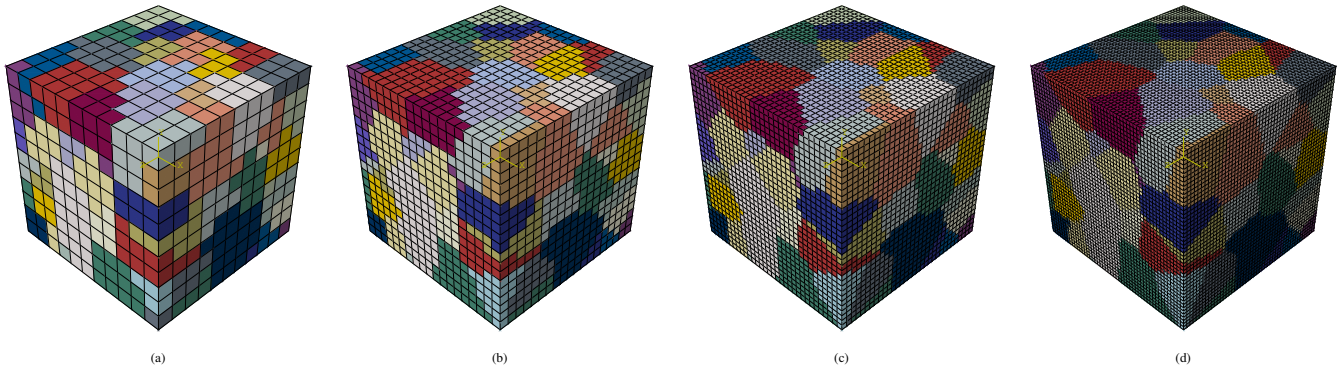

FIGURE 2 Three mesh resolutions with grains represented by different colors. Each mesh has a) $11 \times 11 \times 11$; b) $19 \times 19 \times 19$; c) $32 \times 32 \times 32$; d) $48 \times 48 \times 48$ elements respectively.

Parameter	Value	Parameter	Value
$\dot{\gamma}_0$, 1/s	0.001	r, MPa	0
m, (-)	50	$a_{\text{time=0}}$, MPa	0
τ_0, Mpa	334	h, MPa	500

TABLE 1 Parameters used in crystal plasticity model

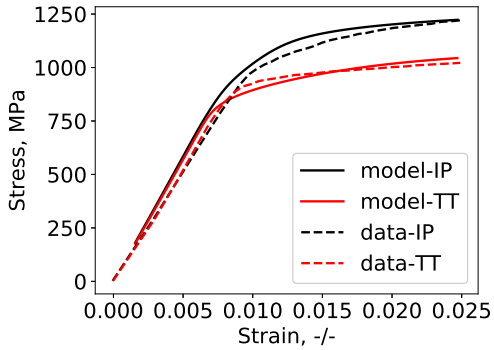

FIGURE 3 Predicted stress–strain curve as compared to the wrought Ti-6Al-4V data in[26] for the in-plane direction (IP) which is parallel to the rolling direction and the through-thickness direction (TT) which is perpendicular to the rolling direction.

3 | RESULTS

3.1 | Comparison to Experiments

Before presenting the statistical spread predictions from the model, the spread observed in Ti-6Al-4V fatigue data is addressed. Since fatigue life is measured experimentally while FIP is calculated by the model, each measured fatigue life is converted to FIP via Eq. 1. To do this, FIP values from all four meshes and all four nonlocal volume average procedures is fit to life data.

For this fitting, a single realization of the microstructure from Fig.6 is simulated for a maximum stress of 586, 600, and 655 MPa and $R = -1$. This realization is chosen to give FIP values in the middle of each of the lowest histogram bin in Fig.6 and is considered to represent the expected FIP value. The simulated FIPs are fit to the best fit line for the fatigue life of a solution treated and aged Ti-6-Al-4V plate (from the MMPDS handbook[18]) in Fig.4. The fitting procedure uses Matlab's `fminsearch` to fit the parameters A and b in $FIP = AN^b$ to the equivalent stress[‡] best-fit line equation from MMPDS. In Fig.4, the difference between the fit fatigue life (N) values for each mesh size and nonlocal volume is negligible even though each A and b value is different. The parameters A and b for

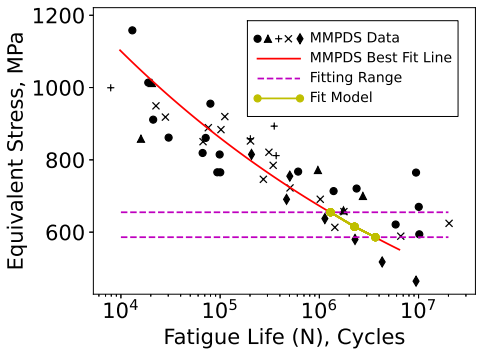

FIGURE 4 Equivalent stress and fatigue life for a Ti-6Al-4V plate cycled at various R ratios: -1 (●), -0.4(▲),0 (+),0.1 (×), 0.3 (♦). The simulated FIP values (in a given fitting stress range) are converted to fatigue life via fitting parameters.

[‡] Equivalent stress as defined by MMPDS is stress "that consolidates data for all stress ratios into a single curve", it is not the von Mises stress.

each mesh size and nonlocal volume are then used to convert the histogram of fatigue life from Fig.4 to FIP values.

The probability density function for FIP values converted from fatigue life using the fitting parameters discussed above are shown in Fig.5. Each fatigue life in the fitting range shown in Fig.4 is converted to FIP to give an estimate of the experientially observed statistical spread in FIP values. For each case, a three parameter Weibull distribution is fit to the probability density function using Python's `scipy.stats.exponweib` function. These Weibull distributions are compared to simulations in Fig.6.

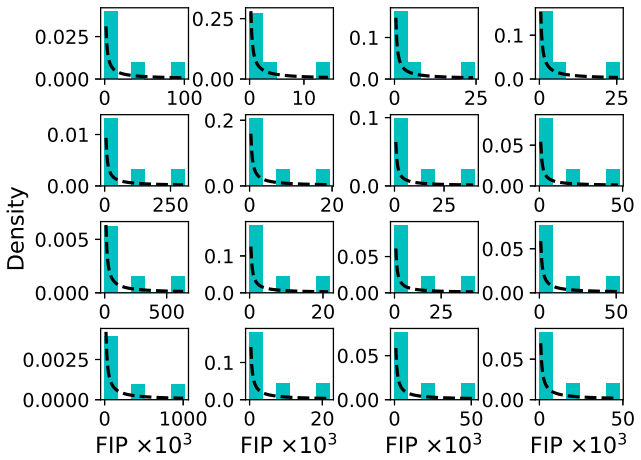

FIGURE 5 The probability density function (i.e., density) for each mesh size and nonlocal volume is shown (by the dashed line) based on the fatigue life in the fitting range in Fig.4. The density is determined from the normalized histograms based on the data.

3.2 | Fatigue Indicator Parameter

Fig.6 shows FIP results using four types of nonlocal volume averages for each of the four mesh sizes (i.e., $11 \times 11 \times 11$, $19 \times 19 \times 19$, $32 \times 32 \times 32$, and $48 \times 48 \times 48$ elements). The local FIP values for each mesh size are the same, but the volume over which these FIPs are averaged and the averaging procedure differs.

FIP values denoted as *element* are not averaged (i.e., the nonlocal volume is only one element). The FIP values denoted as *conformal* use cubic nonlocal volumes that do not overlap (as shown in Fig.1c). The FIP values denoted as *nonconformal* use spherical overlapping nonlocal volumes centered at every element (as shown in Fig.1d); for the *nonconformal* average, every FIP is weighted equally. The FIP values denoted as *weighted* use the same nonlocal volumes as the *nonconformal* average but weight each element's FIP values using Eq. 5.

The error shown in Fig.6 is calculated using

$$e = 100\% \frac{\max\left(FIP^{\text{nl}}_{\text{model}}\right) - \max\left(FIP^{\text{nl}}_{\text{exp.}}\right)}{\max\left(FIP^{\text{nl}}_{\text{exp.}}\right)}, \qquad (13)$$

where e is the error in the model as a percentage (which is negative if the model under-predicts and positive if the model over-predicts FIP values) and $FIP^{\text{nl}}_{\text{model}}$ and $FIP^{\text{nl}}_{\text{exp.}}$ are the nonlocal FIP values from the model and experiments, respectively.

4 | DISCUSSION

As shown in Fig.6, the local *element* value of FIP has a large spread but also a large mesh dependence. For the conformal nonlocal volumes, the mesh dependence is minimal but the spread is limited. For the nonconformal nonlocal volumes, the mesh dependence is also minimal but the spread is wider than the conformal nonlocal volume; albeit not as wide as the element local FIP.

The $48 \times 48 \times 48$ element mesh with the element nonlocal volume average is the only to over-predict the data. All other predictions under-predict the data. For the $32 \times 32 \times 32$ and $48 \times 48 \times 48$ elements meshes the effect of nonconformal nonlocal volumes is the most clear. While the mesh dependent element averages for the $32 \times 32 \times 32$ and $48 \times 48 \times 48$ element meshes show -8% and 25% error respectively, the mesh independent conformal element averages show -76% and -75% respectively. This error is reduced for the mesh independent nonconformal element averages, where for the $32 \times 32 \times 32$ and $48 \times 48 \times 48$ element meshes the error ranged from -16% to -52%. The weighted average shows between 3% and 27% less error than for the nonconformal average; thus, the weighted nonconformal average is considered more accurate than the nonconformal average without weighting.

5 | CONCLUSIONS

A new nonconformal nonlocal volume averaging approach is proposed for FIP and fatigue life calculations based on a similar approach previously used to predict ductile fracture and porosity. Of these nonlocal approaches, the local *element* value of FIP has a large spread but also a large mesh dependence. For the conformal nonlocal volumes, the mesh dependence

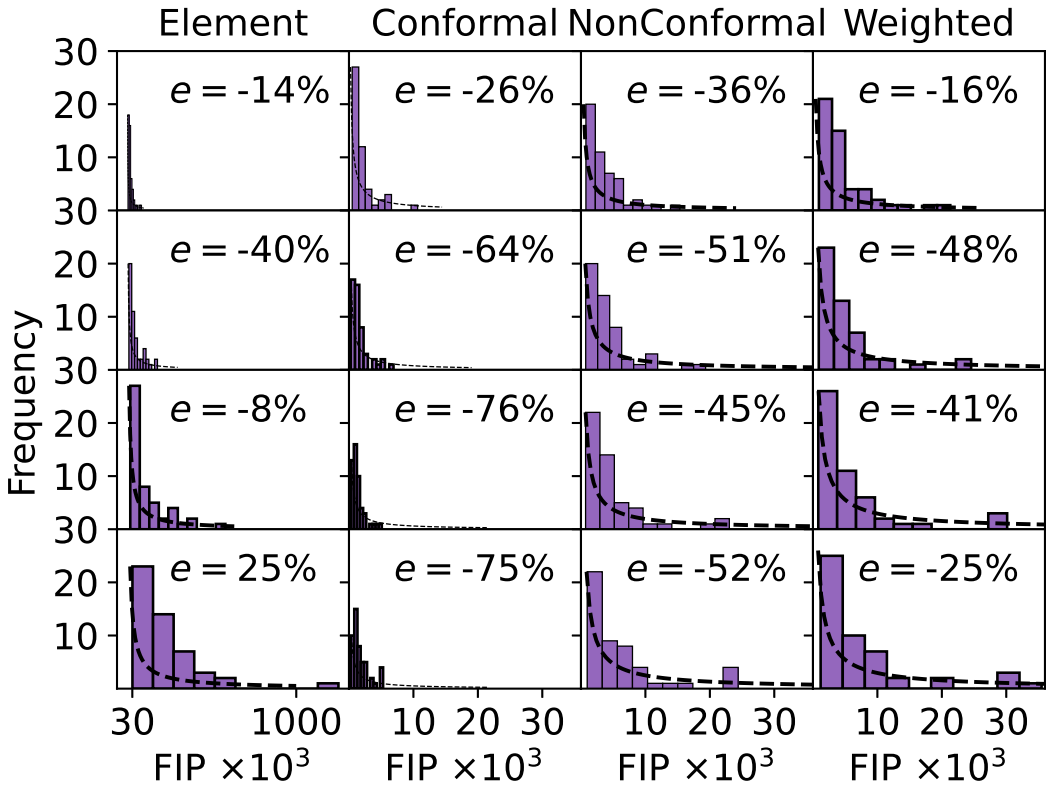

FIGURE 6 FIP for 50 realizations, using a local *element* volume, a *conformal* nonlocal volume, a *nonconformal* nonlocal volume, and a *weighted* nonconformal nonlocal volume. The coarse to fine meshes are top to bottom respectively. The probability density functions from Fig.5 are scaled to the maximum histogram value and shown with dashed lines. The error e is also given (where negative values indicate that the simulation underestimates the data in the probability density functions).

is minimal but the spread is limited. For the nonconformal nonlocal volumes, the mesh dependence is also minimal but the spread is wider than the conformal nonlocal volume; albeit not as wide as the element local FIP.

The error in the spread in FIP values is greatly reduced using the nonconformal approach (as compared to the conformal approach). The error is the smallest for the nonconformal nonlocal volume where the FIP values are weighted when averaged. The two nonconformal approaches better capture the statistical spread in fatigue life seen in Ti-6Al-4V. The spread from the weighed nonlocal volume is larger than for the non-weighted nonlocal volume and more representative of fatigue statistics.

While the MMPDS data are limited both in terms of fatigue life and stress range, the spread in the data from MMPDS is typical of fatigue tests. Also, while there is some overhead to calculating the larger number of nonconformal nonlocal volumes (as compared to the smaller number of conformal nonlocal volumes), this calculation is only for post-processing; it does not need recomputed for each microstructure—only for each mesh—so these volumes are determined once and then are used repeatedly.

Therefore, a weighted nonconformal nonlocal average is computationally tractable and predicts a more accurate statistical spread in FIP values than the other mesh independent nonlocal approaches considered.

ACKNOWLEDGEMENT

This material is based upon work supported by the National Science Foundation under Grant No. Award Number 1934753. Support was provided by the Division of Civil, Mechanical and Manufacturing Innovation's (CMMI) Mechanics of Materials and Structures (MOMS) program. The author's would like to thank Dr. Dinc Erdeniz of the University of Cincinnati for his discussion about and support of this work.

REFERENCES

1. McDowell DL. Simulation-based strategies for microstructure-sensitive fatigue modeling. *Mat Sci Eng A.* 2007;468:4–14.
2. Zhang J, Prasannavenkatesan R, Shenoy MM, McDowell DL. Modeling fatigue crack nucleation at primary inclusions in carburized and shot-peened martensitic steel. *Eng Fract Mech.* 2009;76(3):315–334.
3. Castelluccio GM, McDowell DL. Assessment of small fatigue crack growth driving forces in single crystals with and without slip bands. *Int. J. Fract..* 2012;176(1):49–64.
4. Prasannavenkatesan R, Przybyla CP, Salajegheh N, McDowell D. Simulated extreme value fatigue sensitivity to inclusions and pores in martensitic gear steels. *Eng Fract Mech.* 2011;78(6):1140–1155.
5. Salajegheh N, Prasannavenkatesan R, McDowell DL, Olson GB, Jou HJ. Finite element simulation of shielding/intensification effects of primary inclusion clusters in high strength steels under fatigue loading. *J Eng Mater-T ASME.* 2014;136(3):031003.
6. Moore JA, Frankel D, Prasannavenkatesan R, Domel AG, Olson GB, Liu WK. A crystal plasticity-based study of the relationship between microstructure and ultra-high-cycle fatigue life in nickel titanium alloys. *Int. J. Fatigue.* 2016;91:183–194.
7. Muth A, John R, Pilchak A, Kalidindi SR, McDowell DL. Analysis of Fatigue Indicator Parameters for Ti-6Al-4V microstructures using extreme value statistics in the transition fatigue regime. *Int. J. Fatigue.* 2021;153:106441.
8. Salajegheh N, McDowell DL. Microstructure-sensitive weighted probability approach for modeling surface to bulk transition of high cycle fatigue failures dominated by primary inclusions. *Int J Fatigue.* 2014;59:188–199.
9. Moore JA, Rusch JP, Nezhad PS, Manchiraju S, Erdeniz D. Effects of martensitic phase transformation on fatigue indicator parameters determined by a crystal plasticity model. *Int. J. Fatigue.* 2023;168:107457.
10. Shenoy M, Kumar R, McDowell D. Modeling effects of nonmetallic inclusions on LCF in DS nickel-base superalloys. *Int J Fatigue.* 2005;27(2):113–127.
11. Castelluccio GM, McDowell DL. Microstructure and mesh sensitivities of mesoscale surrogate driving force measures for transgranular fatigue cracks in polycrystals. *Mater. Sci. Eng., A.* 2015;639:626–639.
12. Brown MW, Miller K. A theory for fatigue failure under multiaxial stress-strain conditions. *Proc. Inst. Mech. Eng.,.* 1973;187(1):745–755.
13. Lankford J, Kusenberger F. Initiation of fatigue cracks in 4340 steel. *Metall. Trans..* 1973;4(2):553–559.
14. Shenoy M, Zhang J, McDowell DL. Estimating fatigue sensitivity to polycrystalline Ni-base superalloy microstructures using a computational approach. *Fatigue Fract. Eng. Mater. Struct.* 2007;30(10):889–904.
15. Kumar R, Wang AJ, McDowell D. Effects of microstructure variability on intrinsic fatigue resistance of nickel-base superalloys–a computational micromechanics approach. *Int. J. Fract..* 2006;137(1-4):173–210.
16. Castelluccio GM, McDowell DL. Mesoscale modeling of microstructurally small fatigue cracks in metallic polycrystals. *Mater. Sci. Eng., A.* 2014;598:34–55.
17. Fatemi A, Socie DF. A Critical Plane Approach to Multiaxial Fatigue Damage Including Out-Of-Phase Loading. *Fatigue Fract Eng M.* 1988;11(3):149–165.
18. United States, and Battelle Memorial Institute. MMPDS-01 Metallic Materials Properties Development and Standardization (MMPDS). [Washington, DC]: Federal Aviation Administration, 2008.. https://mmpds.org/; .
19. Leblond J, Perrin G, Devaux J. Bifurcation effects in ductile metals with nonlocal damage. *JJ. Appl. Mech..* 1994;61(12):236–242.
20. Enakoutsa K, Leblond J, Perrin G. Numerical implementation and assessment of a phenomenological nonlocal model of ductile rupture. *Comput. Methods Appl. Mech. Eng..* 2007;196(13-16):1946–1957.
21. *Multiprocessing – Process-based parallelism https://docs.python.org/3/library/multiprocessing.html*. .
22. Dask Development Team . *Dask: Library for dynamic task scheduling https://dask.org*. Dask; : 2016.
23. McGinty R. *Multiscale Representation of Polycrystalline Inelasticity*. PhD thesis. Georgia Institute of Technology, ; 2001.
24. Mayeur J, McDowell D. A three-dimensional crystal plasticity model for duplex Ti–6Al–4V. *Int. J. Plast..* 2007;23(9):1457–1485.
25. Moore JA, Barton NR, Florando J, Mulay R, Kumar M. Crystal plasticity modeling of β phase deformation in Ti-6Al-4V. *Modell. Simul. Mater. Sci. Eng..* 2017;25(7):075007.
26. Mulay R, Moore J, Florando J, Barton N, Kumar M. Microstructure and mechanical properties of Ti–6Al–4V: Mill-annealed versus direct metal laser melted alloys. *Mater. Sci. Eng., A.* 2016;666:43–47.
27. Quey R, Dawson P, Barbe F. Large-scale 3D random polycrystals for the finite element method: Generation, meshing and remeshing. *Comput. Methods Appl. Mech. Eng..* 2011;200(17-20):1729–1745.
28. Quey R, Renversade L. Optimal polyhedral description of 3D polycrystals: Method and application to statistical and synchrotron X-ray diffraction data. *Comput. Methods Appl. Mech. Eng..* 2018;330:308–333.
29. Quey R, Villani A, Maurice C. Nearly uniform sampling of crystal orientations. *Journal of Applied Crystallography.* 2018;51(4):1162–1173.